Aerosol-assisted CVD-grown PdO nanoparticle-decorated tungsten oxide nanoneedles extremely sensitive and selective to hydrogen

Fatima. E. Annanouch[1], Z. Haddi[1,2], M. Ling[3], F. Di Maggio[3], S. Vallejos[4], T.Vilic[1], Y. Zhu[3], T. Shujah[3,5], P. Umek[6], C. Bittencourt[7], C. Blackman[3,] and E. Llobet[1,*]*

[1]MINOS-EMaS, Universitat Rovira i Virgili, Avda. Països Catalans, 26, 43007 Tarragona, Spain

[2] Laboratoire des Sciences de l'Information et des Systèmes (LSIS), Aix-Marseille University, France

[3]Department of Chemistry, University College London, 20 Gordon Street, London, WC1H 0AJ, United Kingdom

[4]SIX Research Centre, Brno University of Technology, Technická 10, Brno, CZ-61600, Czech Republic

[5]GC University, Katchery Road, Lahore 54000, Pakistan

[6]Department of Solid-State Physics, Jožef Stefan Institute, Jamova cesta 39, 1000 Ljubljana, Slovenia

[7]Materia Nova, Univeristé de Mons, Parc Initialis - Av. N. Copernic, 1, B-7000, Mons, Belgium

KEYWORDS: Aerosol Assisted CVD, nanoneedles, nanoparticles, gas sensor.

Abstract

We report for the first time the successful synthesis of palladium nanoparticle (NP) decorated WO_3 nanoneedles (NNs) via two step aerosol assisted chemical vapor deposition (AACVD) approach. Morphological, structural and elemental composition analysis revealed that $Pd(acac)_2$ precursor was very suitable to decorate WO_3 NNs with uniform and well dispersed PdO NPs. Gas sensing results revealed that decoration with PdO NPs led to an ultra-sensitive and selective H_2 gas sensor (sensor response peaks to 1670 at H_2 500 ppm) with low operating temperature (150 °C). The response of decorated NNs is 755 times higher than that of bare WO_3 NNs. Additionally, at temperature near that of the ambient (50 °C), the response of this sensor toward the same concentration of H_2 was 23, which is higher than that of some promising sensors reported in the literature. Finally, humidity measurements showed that PdO/WO_3 sensors displayed low-cross sensitivity toward water vapor, compared to bare WO_3 sensors. The addition of PdO NPs helps minimizing the effect of ambient humidity on sensor response.

Introduction

Tungsten trioxide (WO_3) is an important *n*-type semiconductor with a band gap between 2.4 and 2.8 eV, which has a variety of applications including electrochromic and photochromic devices,[1,2] photocatalysis,[3] and gas sensors.[4] With the development of nanotechnology, WO_3 has been synthesized in different forms such as nanoneedles,[4] nanotubes,[5] and nanorods,[6] which owing to unique properties not possessed by its bulk form, provide intrinsic advantages for the aforementioned applications. For instance in gas sensors, the high surface-to-volume ratio has improved gas sensitivity,[7] and the relatively high level of crystallinity has improved the stability of sensor response.[4] Consequently, nanostructured WO_3 has been used for sensing a variety of gases such as CO, NO_2, NO, H_2, NH_3 etc. Among these gases, hydrogen has recently triggered much interest as a renewable energy source.[8] It is considered as an essential fuel source in clean-energy transportation and power generation applications. Simultaneously, it is colorless, odorless,

tasteless, and highly flammable and explosive at volume concentrations higher than ca. 4%.[9] Thus, there is serious concern regarding its safe production, storage, and transportation.

On the basis of what is reported in the literature,[10,11] the sensitivity of bare nanostructured WO_3 sensors toward hydrogen is not good enough. Additionally, their high working temperatures, long response time, humidity cross-sensitivity and low selectivity make them unsuitable for reliable, robust and accurate H_2 sensors. To overcome these drawbacks, the addition of decorating catalyst nanoparticles onto the metal oxide matrix (i.e., surface functionalization of the nanostructured metal oxide) has been explored, providing demonstrated improvements in selectivity toward a target gas,[7,12] especially, when the size of the host matrix elements is within the Debye length (L_D) and the catalyst nanoparticles are incorporated in small, discrete amounts.[13] Several strategies to modify functionality of the host matrix have been investigated.[14] These fall broadly into two categories, either one-step processes in which the metal nanoparticles (NPs) and metal oxide (MOX) nanostructures are grown simultaneously (e.g. co-deposition via AACVD) or a multi-step approach in which the metal additives are deposited or incorporated on the surface of previously grown metal oxide nanostructures.

It is well known that Pd/PdO nanoparticles have been widely used as a sensitizer in metal oxide films for H_2 gas sensors.[15,16,17] Their incorporation promotes the dissociation of H_2 molecules to hydrogen atoms and thus enhances the electrochemical reactions at the surface or/interface of the metal oxide host matrix. Suematsu and co-workers have synthesized Pd loaded SnO_2 NPs responding to 200 ppm of H_2.[18] The sensors showed a remarkable sensitivity and sensor response (S_R) toward H_2 was equal to 2000, but their optimal working temperature was rather high (i.e., 300 °C). Chang and co-workers have investigated the H_2 gas sensing properties of Pd NP decorated ZnO nanorods.[19] The maximum response (S_R=1371) toward 600 ppm of H_2 was achieved at 260 °C. However the sensing element was produced employing a time-consuming technique that included various wet chemical deposition steps. Chavez and co-workers have reported on the sensing performance of Pd functionalized WO_3 nanowires by drop-casting method.[20] The

fabricated sensors exhibited very small response (3.1) toward high concentration of H_2 (1000 ppm) at a rather high optimal working temperature of 300 °C. It is worth noting that the sensing element of most of the reported works on Pd/MOX sensors was not directly grown onto the sensor substrates, and this is due to the limitations of the techniques adopted during the synthesis. Moreover, WO_3 nanostructures decorated with PdO/Pd NPs have not been widely explored for the detection of H_2, since most of the reported works were focused on the use of SnO_2 as host matrix. Finally, none of the papers cited above reported the effect of ambient humidity on sensor response, yet it is well known that humidity generally diminishes the resistance of an *n*-type semiconductor gas sensor, which results in an interfering effect for the detection of H_2.

Herein we report on the AACVD synthesis of PdO NPs-decorated WO_3 nanoneedles (NNs), onto MEMs based micro-hotplate transducers, using a two-step strategy. To our knowledge, no previous reports have described the synthesis of PdO NPs decorated WO_3 NNs via AACVD method for gas sensing application. Scanning electron microscopy (SEM), X-ray diffraction (XRD), transmission electron microscopy (TEM), high-resolution TEM (HRTEM), and X-ray photoelectron spectroscopy (XPS) have been used to determine the morphology, phase composition, and microstructure of the deposited layers. Their gas sensing performances toward detecting H_2 have been investigated in both humid and dry atmospheres. Furthermore, CO, NH_3, C_6H_6 and moisture have been used as interfering species in order to study the sensors' selectivity. Finally, the sensing mechanism for H_2 in PdO NPs decorated WO_3 NNs is discussed as well.

Experimental section

MEMs transducer platforms. MEMS-based microsensor platforms were implemented in a double side polished p-type <100> Si substrates with a 300 μm thickness. Clean room processes were carried out at the wafer level and consisted of the following microfabrication steps including implantation, photolithography, metallization, lift-off and rear side etching of the substrate to define the membranes. In one chip, four membranes with dimension of 1 mm × 1 mm, were

grown via LPCVD (Low-pressure CVD) technique. Each membrane (see Figure 1) comprised of a $POCl_3$-doped polysilicon meander shaped resistive heater (16 Ω/sq, 0.47μm thickness, and a temperature coefficient of resistivity (TCR) equal to 6.79×10^{-4}/ºC), silicon oxide insulator layer (800 nm thick), and platinum electrodes (0.2 μm thickness, 50 μm electrode gap). Each chip consisted of an array of four microsensors bounded and mounted on a standard TO-8 package.[7] It is worth noting, that during AACVD deposition, a shadow mask was used to avoid contact between the heater and the electrodes pads (contacts) and to confine the film deposition to the electrode area.

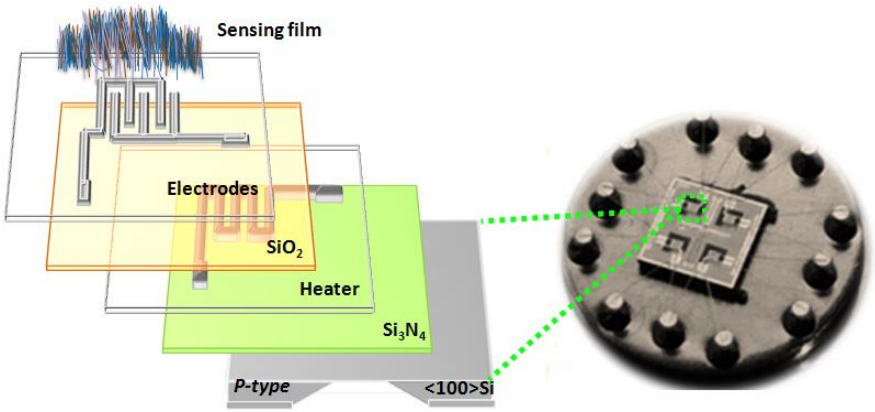

Figure 1. schematic view of the layers comprising the MEMs based gas microsensors.

Reactants. Palladium(II) acetylacetonate ($Pd(acac)_2$) (99 %), Tungsten hexacarbonyl (97 %), Methanol (≥99.9%), Ethanol (≥99.8%) and Acetone (≥99.9%) were obtained from Sigma-Aldrich and were used as received without further purification.

Procedure. Synthesis of Pd nanoparticle decorated WO_3 nanoneedles. Depositions were carried out in a horizontal hot wall AACVD reactor using N_2 (g) (99.96%, BOC) as a carrier gas. A Johnson Matthey Liquifog 2 operating at 2 MHz was used to generate the aerosol from the precursor solutions. MEMs based microsensors substrates were cleaned with acetone and then

with ethanol, dried with air and then placed inside the reactor. Pure WO_3 NNs were obtained at 500 °C, from AACVD of $W(CO)_6$ (50 mg) dissolved in a mixture of acetone (15 cm^3) and methanol (5 cm^3). Conditions were chosen to promote formation of nanostructured WO_3, as described previously,[21] on the MEMS platforms. We have previously explored the relationship between WO_3 NNs dimensions and sensing properties [22,7] with the growth conditions used providing NNs with dimensions consistent with optimum performance as identified in those articles. Pd nanoparticle decorated WO_3 nanoneedles were prepared via a two-step AACVD method. In the initial stage pure WO_3 NNs were deposited, followed by annealing at 500 °C for 3 hours in air. In the subsequent step, palladium nanoparticles were incorporated on the pre-grown nanoneedles via AACVD of $[Pd(acac)_2]$ (1.5 mg) dissolved in methanol (10 cm^3) at 400 °C. It has been shown previously that sensing performance in Pd/SnO_2 samples improves with decreasing Pd particle size.[23] The value of Pd loading chosen for use on the MEMS platforms was guided by results showing that reducing the amount of Pd precursor reduced the size of Pd NPs (Table S1 and Figure S1 in the Supporting Information, SI). As a note to us - by setting this parameter it is therefore not realistic to vary the Pd loading as that is not the only variable that changes - the particle size also changes, so by selecting for smallest particle size we 'set' the Pd/W ratio.

The nitrogen (99.4%, purchased from BOC, Ltd.) carrier gas flow was maintained at 300 sccm. The deposition time (the time required for all the precursor solution to be transported) was between 25 to 45 min. After synthesis, the reactor was cooled by using the water jacket system (i.e. water cooling system) and all samples were subjected to annealing at 500 °C for 3 h in air.

Material analysis. Scanning electron microscopy (SEM) images were taken using the FEI Quanta 600. XRD patterns were collected by Bruker, AXD D8-Discover, using Cu K-α radiation operated at 40 kV and 40 mA. High resolution transmission electron microscopy (HRTEM) images were performed using a JEOL JEM-2100 with a LaB_6 filament at an acceleration voltage of 200 keV. Images were recorded on a Gatan Orius charge-coupled device. Film samples were prepared by removing the film from the glass substrate via sonication in methanol for 15 min, and then drop-casting onto an Agar Scientific 400 Cu mesh holey carbon grid. Excess solutions were removed with filter paper. XPS analysis of the films was carried out using a Thermo Scientific Kα spectrometer with Al K-α radiation, a dual beam charge-compensation system, and constant pass energy of 50eV. Survey scans were collected in the range 0–1350 eV (binding energy). High resolution peaks were carried out for the principal peaks of W (4f), Pd (3d), C (1s) and O (1s). All the XPS data were elaborated using Casa XPS v.2.3 software and binding energies were referenced with respect to the C 1s peak at 284.5 eV.

Gas sensing tests. Gas-sensing tests were carried out in a Teflon/ stainless steel test chamber (2×10^{-2} dm^3) under a continuous gas flow of 200 sccm. The resistance change of the different samples, while exposed to different concentrations of the studied gases and vapors, was monitored by using an Agilent-34970A multimeter. The desired concentrations of the test gases were obtained by employing calibrated gas bottles and PC-driven mass flow controllers (Bronkhost Hitech 7.03.241). Humidity measurements were performed using an Environics series 4000, which allowed us to automatically mix up to three individual gases in a balance gas (air, pollutant gas, and humidity). The sensors (4 PdO-decorated WO_3 NN sensors and 4 bare WO_3 NN sensors) were exposed to the test gas for 10 min, and subsequently the chamber was purged with air for 30 min, which enabled recording the recovery of their baseline resistance.

After this process, the sensors were ready for a new measurement. The sensor response (R) was defined as R = Ra/Rg for reducing gases and R = Rg/ Ra for oxidizing gases, where Ra and Rg are the sensor resistances at the stationary state in air and after 10 min of exposure to the analytes, respectively.

Results and discussion

Materials Characterization. Bare and decorated WO_3 NNs were successfully grown and directly integrated onto MEMs based gas sensor substrates. The color of all as-deposited films was dark blue indicative of partially reduced tungsten oxide (i.e., WO_{3-x}), while after annealing samples for 3 hours in air; their color changed to white-yellow, indicative of full oxidation of tungsten oxide NNs.[24] SEM imaging of either bare or decorated WO_3 NNs revealed the formation of a thick layer of nonaligned nanoneedles, distributed homogenously over the electrode area (Figure 2a,b,c). The diameter of the nanoneedles was between 50 to 200 nm, while their length was about 19 μm (see Figure 2d).

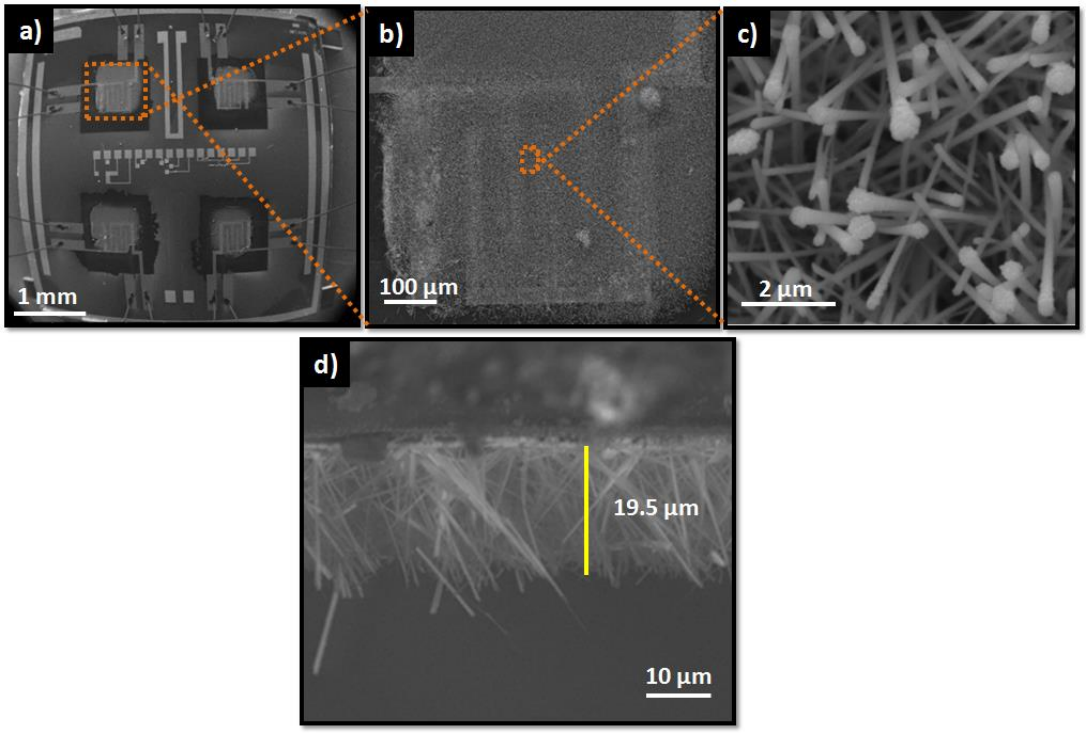

Figure 2. Film morphology observed by SEM images at low (a, b) and high (d) magnification. Cross section of WO_3 nanoneedles (d)

XRD patterns (Figure 3) recorded from undecorated and decorated samples suggested the formation of monoclinic-phase WO_3 NNs (P21/n (14) space group, with typical cell parameters of a=0.729 nm, b=0.7539 nm, c=0.7688 nm, and β=90.91°; ICCD card no. 72-0677), with preferred orientation in the (002) direction for Pd/WO_3 NNs, showing an intense diffraction peak at 23.10° 2θ. No peaks for palladium or palladium oxides were observed in the pattern, likely due to their small size (nanoscale) and/or to the relatively low amount present. The platinum and boron nitride (BN) diffraction peaks indicated in the patterns come from the electrodes and the membrane, respectively.[25] By comparing the patterns of bare WO_3 NNs with the ones of Pd decorated sample, we did not observe any shifts in the WO_3 peak positions demonstrating that the monoclinic crystal structure of tungsten trioxide was not changed during the addition of palladium.

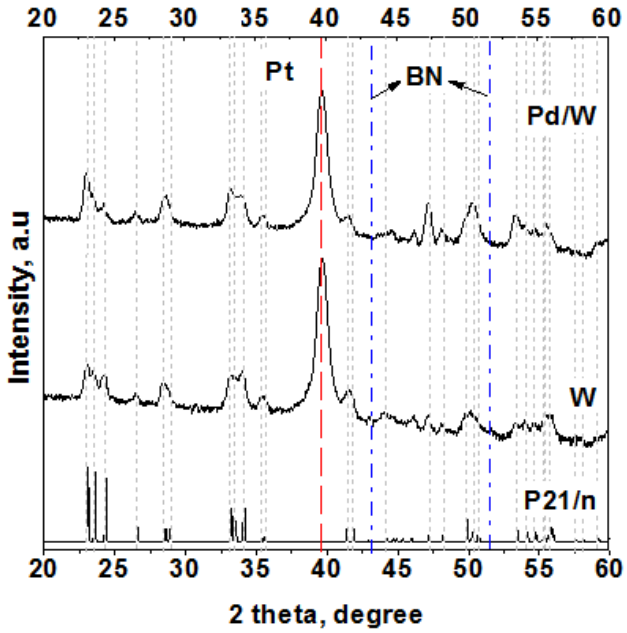

Figure 3. XRD patterns of undecorated and decorated WO_3 NNs deposited at MEMs based gas sensor substrates.

In order to obtain more detailed information about the morphology and the elemental composition of the as-deposited samples, TEM and HRTEM were carried out. In this work, we do not show the HRTEM and XPS results obtained from the pure WO_3 film because they were similar to the ones reported in our previous works.[11,26] Figure 4 shows representative TEM images of the as-deposited NNs decorated with Pd nanoparticles. The results revealed the presence of well-dispersed nanoparticles along the surface of the NNs, consistent with results previously seen for gold and platinum NP functionalized WO_3 NNs.[11]

Overall, the obtained NNs are single crystalline with uniform lattice structures. The spacing between adjacent lattice fringes is 0.378 nm, consistent with the unit cell (c=0.7688 nm) observed by XRD and with our previous results.[26]

On the other hand, Pd NPs displayed approximately spherical morphology, with sizes between 2–4 nm (total measured population was 20 particles). They were characterized by lattice fringes

with interplanar spacing of 0.225 nm corresponding to the (111) plane of face-centred-cubic (fcc) palladium (ICDD card no. 00-046-1043). Thus, TEM and HRTEM results confirm the successful synthesis of Pd nanoparticles via a two-step AACVD route.

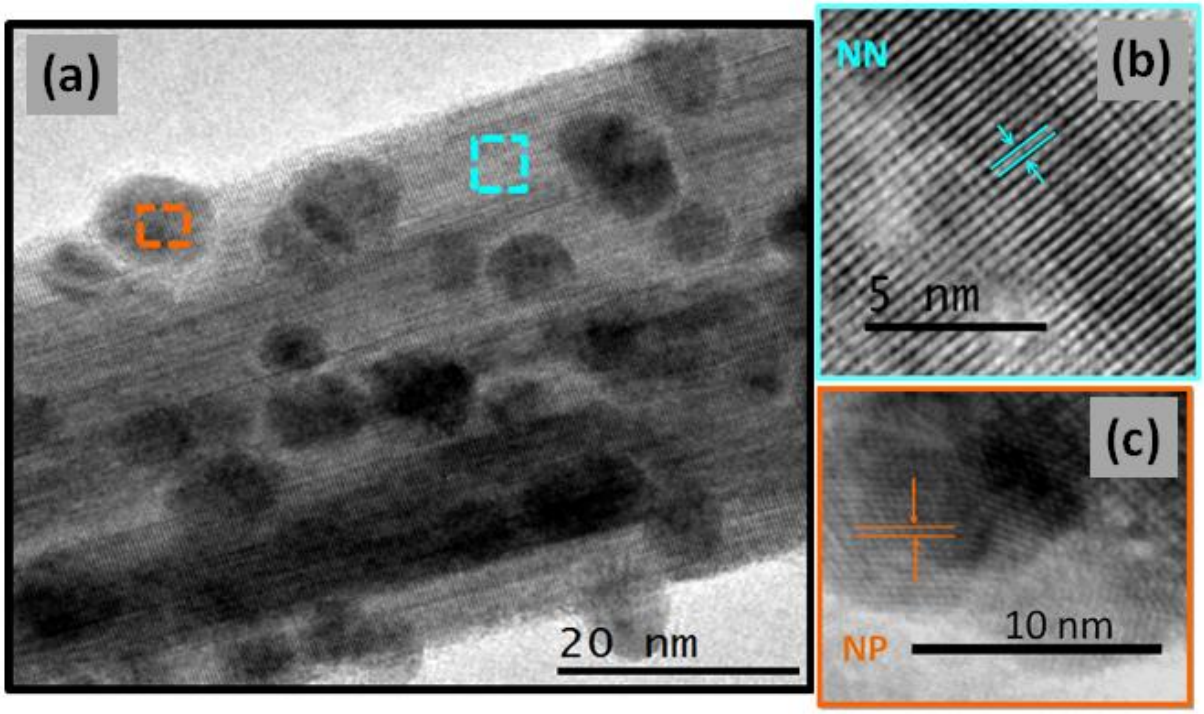

Figure 4. (a) TEM image of as-deposited Pd NPs decorated WO_3 NNs, (b) HRTEM images of WO_3 NNs and (c) Pd NPs. The color code of the insets corresponds to the areas indicated in the TEM image from which the high resolution images were taken.

XPS analysis of the as-deposited and annealed films was conducted. Examination of the W 4f core level spectrum of as-deposited Pd/WO_3 film (Figure 5a) revealed the presence of two intense peaks centered at 35.4 eV and 37.5 eV, which are associated to the W $4f_{7/2}$ and W $4f_{5/2}$ doublet respectively and their values are in good agreement with those found in the literature for W6+ in stoichiometric WO_3 films.[27] The weak emission located around 41 eV is originating from W $5p_{3/2}$ core level. After annealing of the sample, no shifts in the peaks binding energies were observed and the composition of the surface remains stoichiometric (Figure 5b).

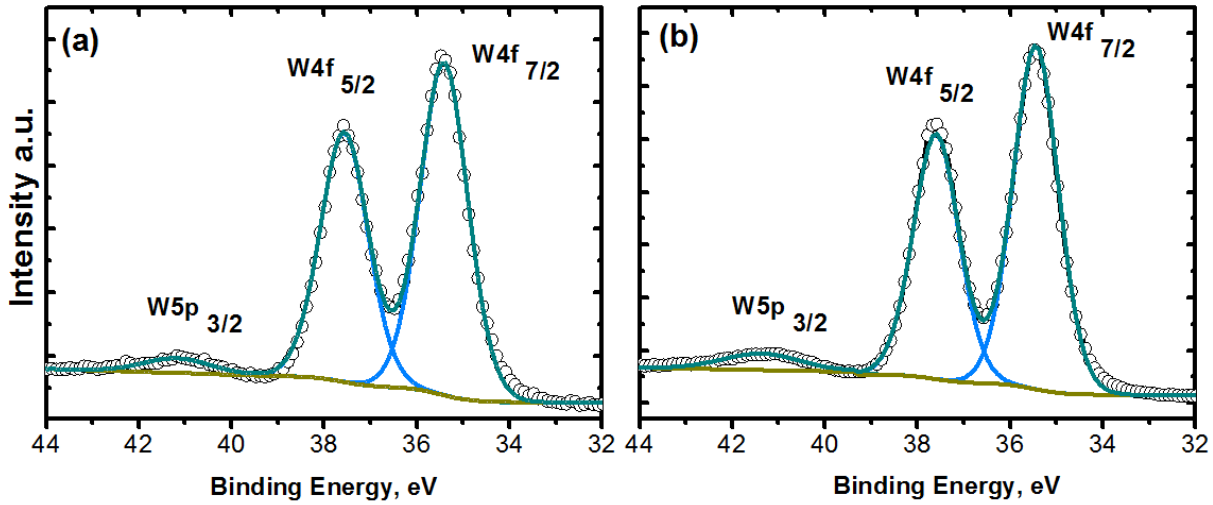

Figure 5. XPS W 4f core-level spectra of (a) as deposited Pd/WO_3, (b) after annealing.

Figure 6a displays the 3d XPS spectra recorded from as-deposited Pd/WO_3 film. This could be fitted by using two deconvoluted doublets. The more intense one, with components centred at 335.1 eV and 340.4 eV, is associated to Pd $3d_{5/2}$ and Pd $3d_{3/2}$ for Pd metal respectively.[28] The low intense one, corresponds to a plasmon loss peak at binding energy of 343 eV and to residual spectral intensity at binding energy of 337.9 eV that may indicate the presence of some sub-oxide (3% or less), although this last assignment is uncertain.[29] After annealing at 500 ºC for 3 h, the XPS spectra of the sample (Figure 6b), was dominated by two peaks at 337.1–342.4 eV,[30] which are ascribed to Pd $3d_{5/2}$ and Pd $3d_{3/2}$ for PdO. Furthermore, HRTEM of the sample after annealing confirmed the presence of PdO, rather than Pd, NP with lattice spacing consistent with the (110) and (101) planes of PdO (0.21 and 0.26 nm respectively, see Figure S2 in the Supporting Information, SI). Hence, for as deposited coatings, the samples consisted of a Pd metal. In contrast, after the annealing, all Pd nanoparticles were oxidized to Pd(II) (i.e., PdO).

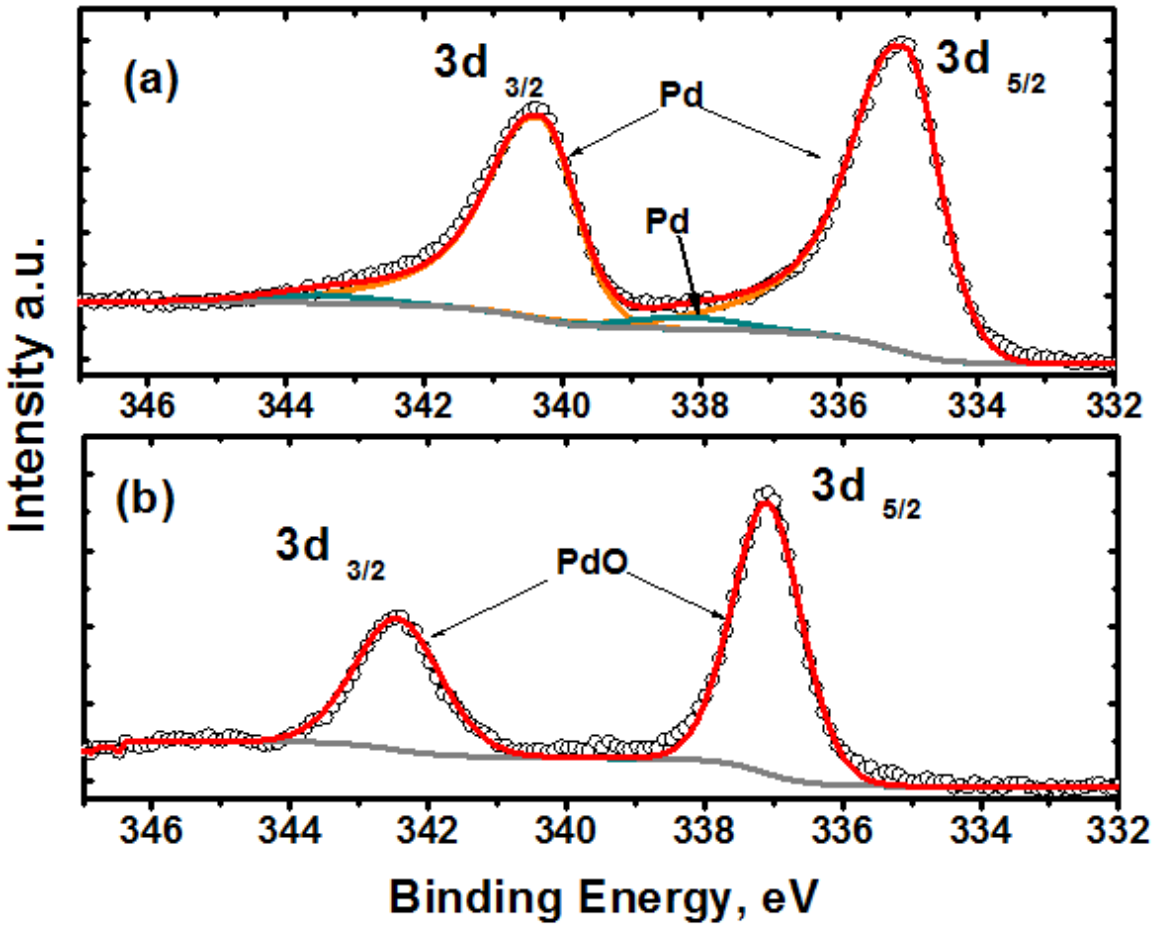

Figure 6. XPS Pd 3d core-level spectra of (a) as deposited Pd/WO_3 and (b) after annealing.

Gas-Sensing Response. Gas sensing tests were carried out to different concentrations of hydrogen by using dc resistance measurements. Undecorated and PdO decorated WO_3 NNs sensors were tested at various temperatures from 50–350 °C, in intervals of 50° C, in order to understand the effect of the temperature on the sensor responses. Four replicate measurements per temperature were performed in order to assess the reproducibility of results. Figure 7 displays the sensor responses to 500 ppm of H_2 as a function of the operating temperature. At temperatures below 200 °C, pristine WO_3 NNs exhibited almost no resistance change, especially at 50 °C and 100 °C, where they were not able to detect the analyte. In contrast, at temperatures exceeding 200 °C, the sensor showed good responses, their maximum (S_R=2.21) toward 500

ppm of H_2, was achieved at 250 °C. This finding indicates the normal behavior known in pure metal oxide sensors, since they need elevated working temperatures. Regarding PdO/WO_3 sensors, the response was increased by increasing the operating temperature, reaching the maximum (S_R= 1670) at 150 °C, then response started to decrease by further increasing the temperature. It was noticeable that below 200 °C, responses were stable and saturated, but above this value, they became small and somewhat unreproducible. This is in agreement with the volcano shape of response intensity as a function of operating temperature observed in metal oxides. The initial increase in response results from an increase in the rate of surface reaction with temperature, and the decrease observed when temperature is further increased results from a decrease in the utility of the gas sensing body (i.e., gas molecules are not able to diffuse onto the whole nanoneedle film).[17,33]

Therefore, 150 °C and 250 °C are the optimal working temperatures for decorated and undecorated WO_3 NN sensors, respectively. They will be adopted for all the investigations hereinafter. Decoration with PdO nanoparticles promotes an increase in sensor response (S_R) as well as a shift of the response maximum towards lower operating temperatures. The sensor becomes able to detect the studied analyte at very low temperature. For instance, at 50 °C, the response of PdO/WO_3 sensor toward 500 ppm of H_2 was equal to S_R = 23, which is significantly higher than that of some promising devices recently reported in the literature.[17,19]

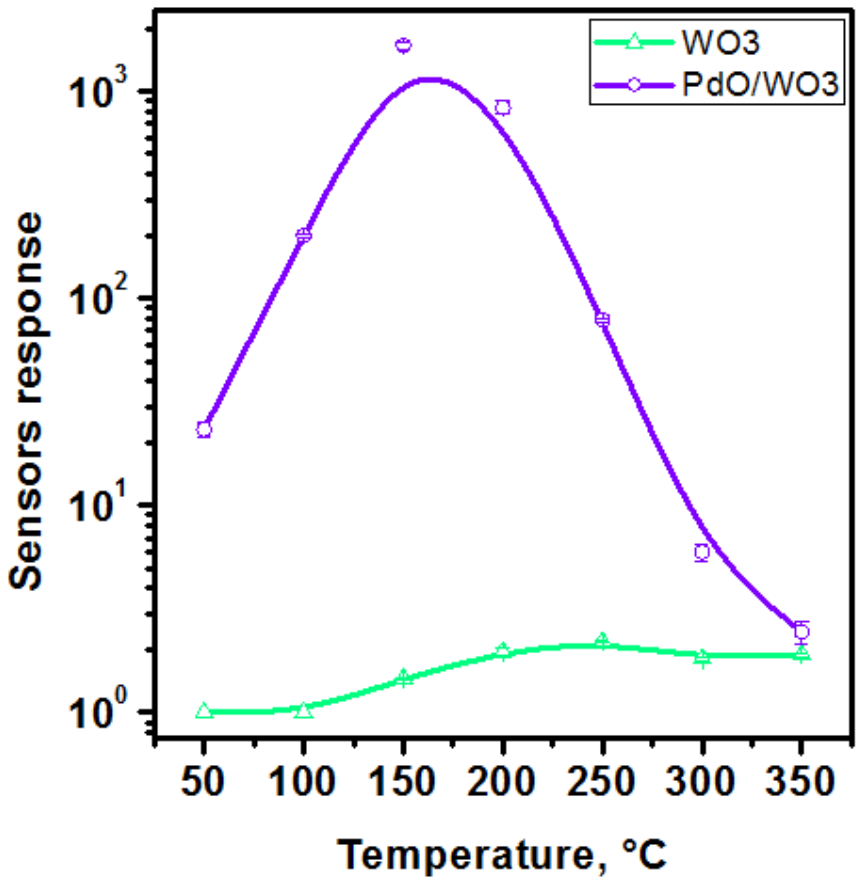

Figure 7. Sensor responses to 500 ppm of hydrogen as a function of operating temperature.

Figure 8 illustrates the change in resistance of undecorated and PdO decorated WO_3 microsensors, toward H_2 pulses with concentrations ranging from 40 to 500 ppm, at their optimal working temperatures. The sensors showed an *n-type* semiconductor behavior, i.e. decreasing electrical resistance when exposed to a reducing gas such as H_2. Furthermore, the sensors showed stable responses with complete recovery of the baseline resistance. It is clear from the graphs that sensors decorated with PdO NPs exhibited the largest resistance change toward H_2 concentrations. Moreover, we have studied the reproducibility of the sensor responses by re-exposing them to 80 ppm of H_2. As it is shown in (Figure 8), the sensors showed reproducible behavior, getting good reproducible responses to 80 ppm of H_2 at the beginning and at the end of

the repeated detection/recovery cycles. In addition, it can be noticed that decorating WO_3 NNs with PdO NPs results in an increase in the baseline resistance. PdO is a well-known *p-type* semiconductor,[31] and WO_3 is an *n-type* semiconductor; thus, *p-n* junctions are formed at the interfaces of the PdO/WO_3 nanocomposite. The formation of these, leads to the occurrence of a space charge layer around each PdO/WO_3 interface, which decreases the free electrons in the conduction band of WO_3 NNs and, therefore, increases the baseline resistance of the sensor.[32,4]

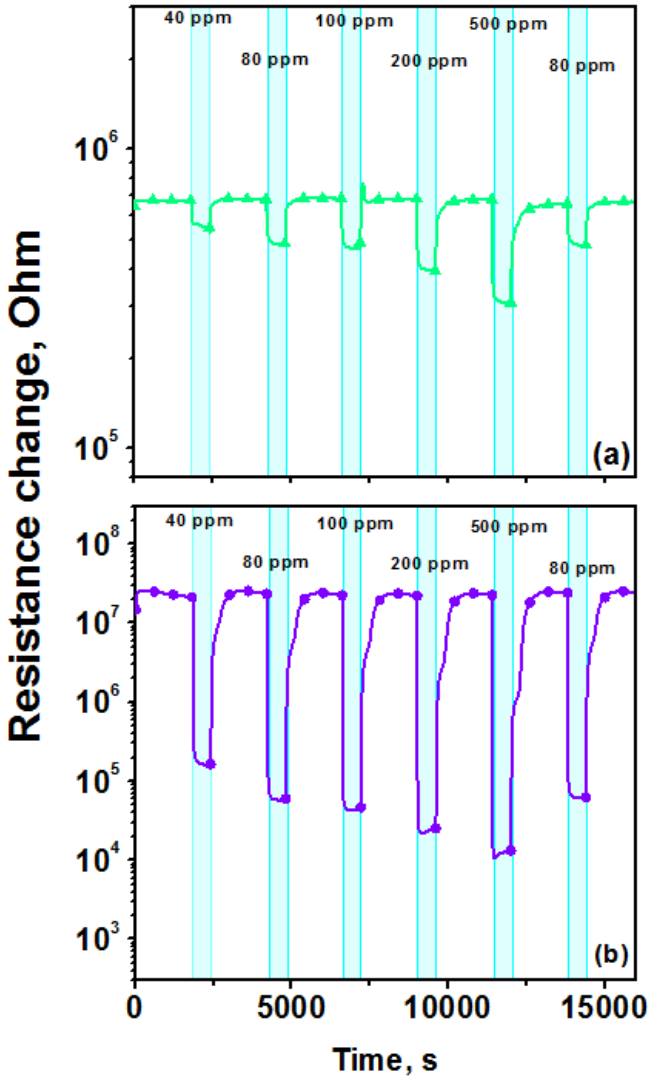

Figure 8. Film resistance changes (a) pristine WO_3 and (b) PdO/WO_3 film toward various concentrations of H_2.

The corresponding gas-sensing response calculated from the change in resistance of undecorated and PdO decorated WO_3 NNs are plotted as a function of H_2 concentration as shown in Figure 9. As we can see, decoration with PdO has greatly enhanced the sensitivity of WO_3 NNs toward H_2. At 500 ppm of H_2, the response of PdO/WO_3 NNs was 755 times higher than that of pure WO_3 NNs. Besides, by increasing the gas concentration the responses of all the sensors were increased. The slope of the calibration curve (i.e. sensitivity) for pure WO_3 sensor was very small compared to the decorated sensor. The response of undecorated sensors varied between 1.23 and 2.21 for concentrations ranging from 40 to 500 ppm of H_2.

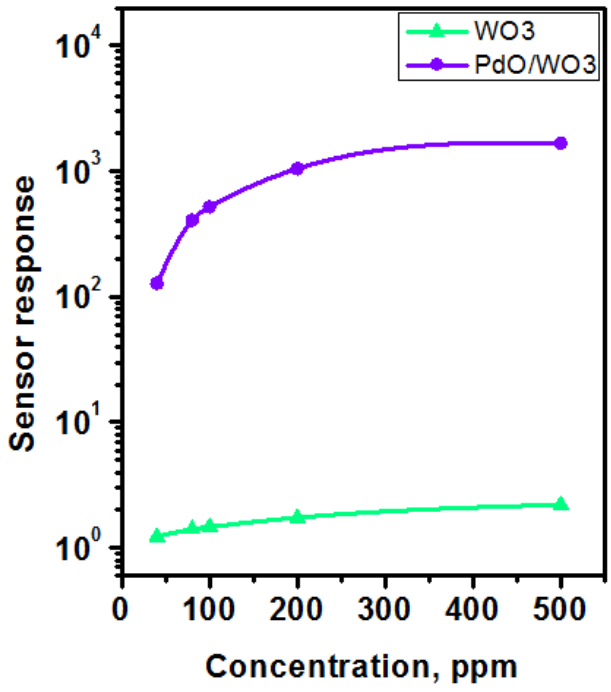

Figure 9. Sensor responses toward various concentration of hydrogen.

The selectivity of bare and PdO decorated WO_3 sensors toward 100 ppm of H_2 was studied by measuring the response to different interfering gases such as NH_3 (100 ppm), C_6H_6 (200 ppm) and CO (200 ppm), at their optimal working temperatures. All these concentrations are chosen with the aim to be higher or equal to the concentration of the target gas (100 ppm of H_2). As

shown in Figure 10a, it is clear that pure WO_3 suffers from a very high cross-sensitivity toward all the interfering gases. In contrast, PdO decorated WO_3 sensor exhibits higher sensitivity toward H_2 (100 ppm) than to the higher concentrations of the interfering gases (Figure 10b). The response of this sensor toward 100 ppm of H_2 is almost 263 times higher than to NH_3 100 ppm, 500 times higher than to C_6H_6 200 ppm, and 463 times higher than to CO 200 ppm. Hence, decoration with PdO NPs has highly enhanced the selectivity of WO_3 NNs toward H_2.

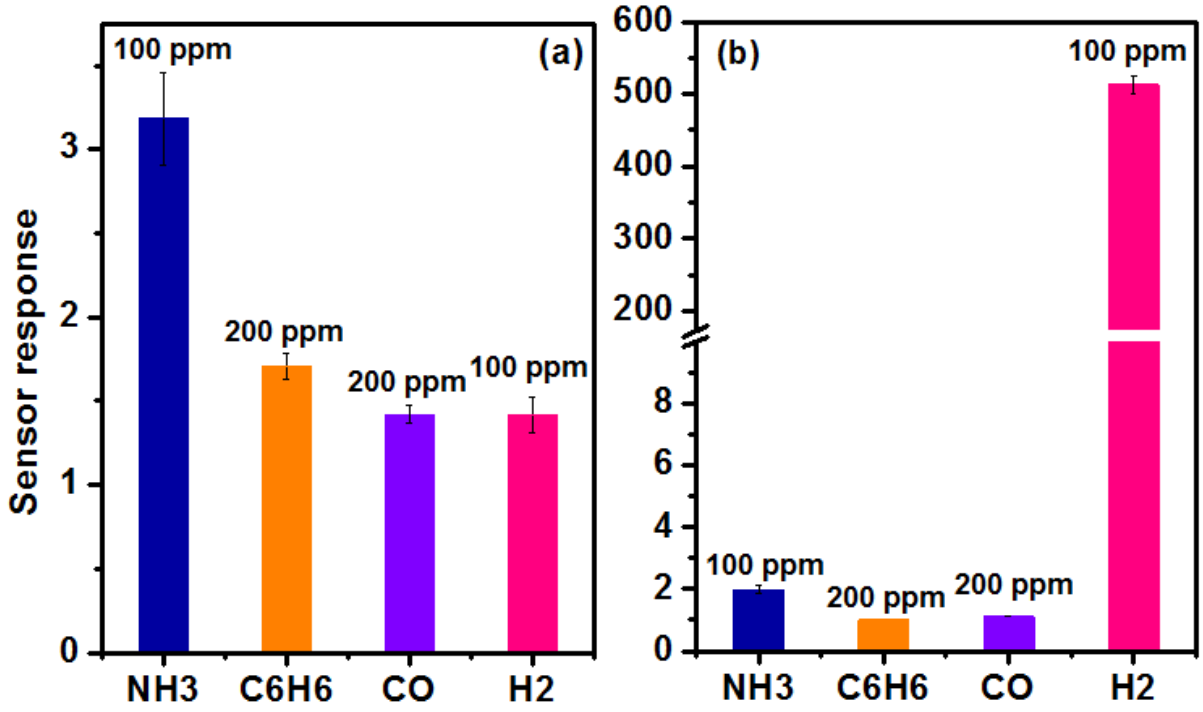

Figure 10. Selectivity diagram of (a) pristine WO_3 and (b) PdO/WO_3 sensors, toward NH_3, C_6H_6 and CO interfering gases.

Mechanism of sensitization by PdO nanoparticles.

The hydrogen sensing of PdO NPs decorated WO_3 NNs can be explained by the interplay of different mechanisms that depend on the working temperature.

Based on the literature, we have found that at temperatures exceeding that of the ambient, the sensitization mechanism of Pd/PdO NPs can be in general associated to *electronic sensitization* and *chemical sensitization* (see Figure 11a). Electronic sensitization occurs due to the presence of PdO NPs, which behave as *p*-type semiconductors. PdO NPs are strong acceptors of electrons from the *n*-type WO_3 NNs and expand the electron depletion layers at the interfaces of the *p*-*n* heterojunctions, which increases the baseline resistance.[4] When H_2 is in contact with PdO NPs and the operating temperature is clearly above room temperature, the hydrogen molecule dissociates into H^+, which results in electronic charge transfer from the PdO NPs towards the WO_3 NNs, and in the relaxation of the space charge layer. Consequently, the electronic conductivity in the WO_3 NNs is raised.[33] In chemical sensitization, PdO NPs both facilitate the increase in the number of oxygen adsorbates present on the surface of WO_3 NNs and favor, via spill-over effect, that H^+ species diffuse onto the surface of the nanoneedles where they further react with oxygen adsorbates.[33,34] To date, there is no clear evidence of which of these mechanisms is more useful for gas sensing, although the literature points to the need to combine both mechanisms to induce an overall better functionality of metal oxide gas sensors. It is the well-known property of Pd and PdO catalyst nanoparticles to dissociate molecular hydrogen and generate H^+ species, which can easily diffuse within the host metal oxide film and are highly reactive, what explains the very high response to hydrogen of PdO-WO_3 NN sensors in comparison to the significantly lower response observed for other reducing species such as CO, NH_3 or C_6H_6.[35]

On the other hand, when the operating temperature is low ($\leq$ 50 °C), Chang and co-workers[19] report that the sensing mechanism is generally related to the dissociation of H_2 molecules over the PdO NPs, and the dissolution of atomic hydrogen in the PdO NPs, forming a palladium

hydride (PdH_x) (see Figure 11b). This has a reduced work function compared to Pd/PdO NPs, and thus facilitates the transfer of charge carriers from the NPs to the host matrix (i.e. the WO_3 NNs).[36] Evidence on the formation of PdHx has been shown by the XPS spectra recorded from the active layer after H_2 measurement, at operating temperature near the ambient (≤ 50 °C) (Figure S3 in the Supporting Information, SI). It is worth noting that at this low temperature, the amount of adsorbed oxygen is intensively diminished since the oxygen spill-over effect is a thermally activated event.[37] Consequently, this mechanism could explain why our PdO NP decorated WO_3 NNs still show a remarkably high response to H_2 when operated at 50ºC.

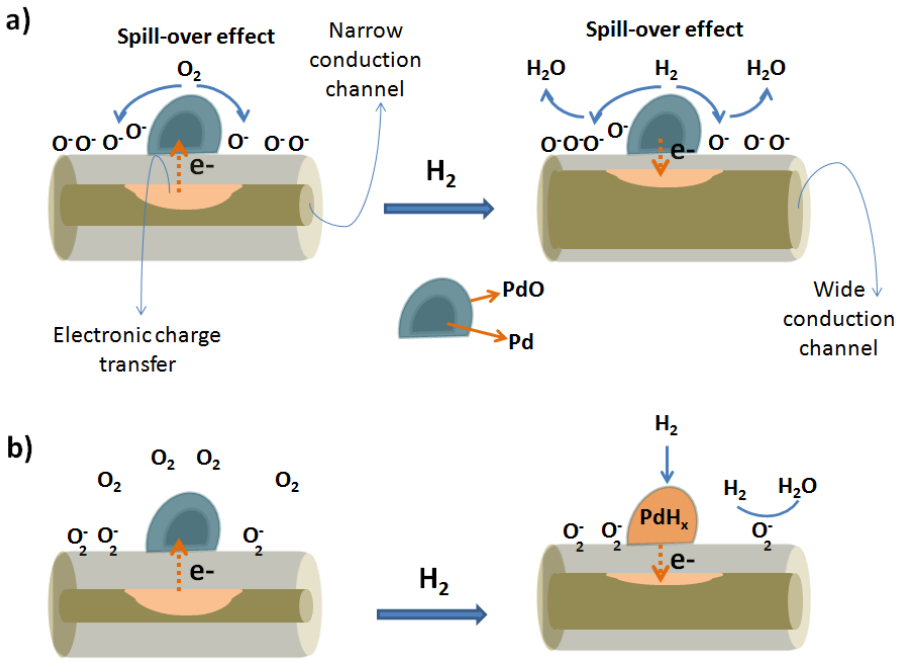

Figure 11. Mechanism of WO_3 sensitization by PdO nanoparticles toward H_2, (a) at operating temperature clearly exceeding that of the ambient and (b) at operation temperature equal or lower than 50 °C.

Humidity effects

Gas sensors are usually intended for detecting target gases in the ambient atmosphere. It is well known that water vapor can affect the sensor response by decreasing its electrical resistance in a similar way as a reducing gas, resulting in an interfering effect for gas detection. Thus it is necessary and compulsory to test the fabricated sensors in a humid background. Figure 12 displays the change in resistance of undecorated and PdO decorated sensors, toward 500 ppm of H_2, under dry or humid (50% relative humidity (RH) at 25 °C) atmospheres. From Figure 12a, it is clear that pure WO_3 is significantly influenced by the presence of humidity. Its baseline resistance decreases by about 55% when humid air is introduced. Additionally, after removing this later, the baseline resistance could not be recovered to its initial value as in the beginning of the measuring cycle. In contrast, PdO/WO_3 sensor (Figure 12b) is only slightly influenced by the presence of humidity. Besides, the sensor could easily recover to its initial state when humidity was removed.

Based on the literature, decoration with Pd/PdO nanoparticles is an effective way to suppress the water vapor cross-sensitivity. Recently, Ma and co-workers showed that adsorbed oxygen species on the surface of Pd-SnO_2 were not influenced by the presence of water vapor.[38] Additionally, they found that the electron depletion layer resulting from the *p-n* junctions present in PdO-SnO_2 may impede OH^- adsorption. Koziej and coworkers suggested that the dispersed Pd NPs at an atomic level on the SnO_2 surface could provide initial adsorption sites for oxygen species and then minimize the effect of the water molecule on the Pd-SnO_2 surface.[39] Thus, the results obtained from decorated sensor in a humid background can be related to the low operating temperature (150 °C). It has been reported that the influence of background humidity can be significant when sensors are operated at low temperatures (< 200 ºC). The adsorption of

the OH-group at the surface of the metal oxide is very strong and needs high operating temperatures to be removed.[40]

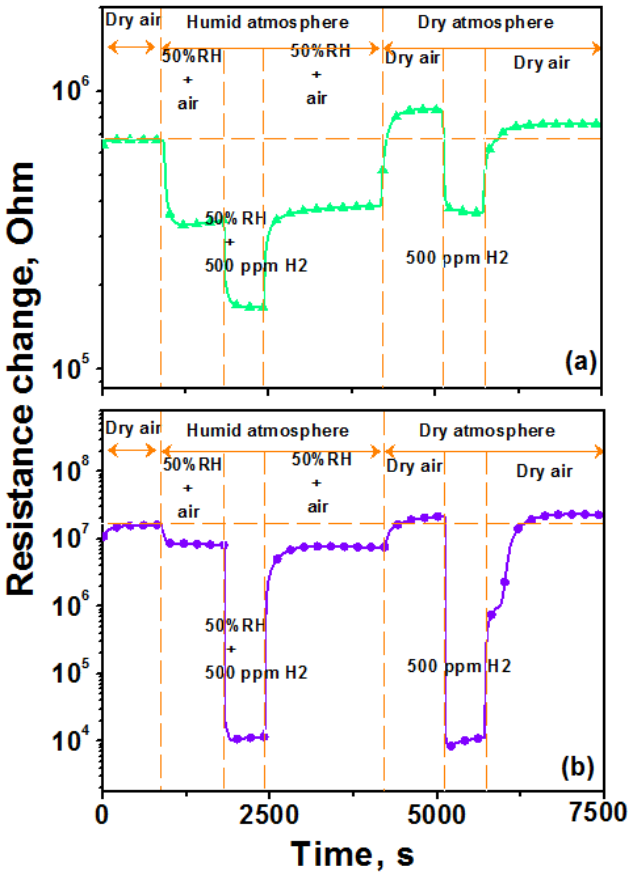

Figure 12. Change in resistance of (a) pristine WO_3 and (b) PdO/WO_3 sensors, toward 500 ppm of H_2, at the presence of both dry and humid (50% relative humidity (RH) at 25 °C) atmospheres.

After gas sensing measurements, sensors based on undecorated and PdO decorated tungsten oxide NNs underwent SEM and XRD analysis, showing no changes either in the morphology or in the structure of both sensing films (see Figure S4, S5 and S6, in the SI). These observations suggest that the sensing material grown directly onto the MEMS platforms remains stable after the temperature changes and the exposure to analytes undergone during the tests.

Table 1 represents a comparative analysis of some characteristics of H_2 sensors based on Pd/PdO nanoparticles decorated metal oxide nanostructures reported in this work and in the literature. We can observe that the response of PdO decorated WO_3 NNs is much higher than those of other Pd decorated metal oxide nanostructures including nanoparticles, nanorods, nanowires and nanofibers. Besides, this higher response is obtained at quite low operating temperatures (i.e. 150 °C). Moreover, more than three-step deposition techniques were employed in the majority of these works to produce the nanocomposite film. In contrast, in our case, we used a two-step AACVD route, which allowed us the direct growth of the nanocomposite film onto the MEMS transducer substrate, within 180 minutes. Finally, by comparing our sensor with the other Pd/WO_3 nanostructures produced by different methods, it is clear that H_2 gas sensing performances are highly dependent on the morphological structure and the preparation method of the Pd NPs decorated WO_3 sensing layer. Consequently, using a simple, scalable and low cost technique (AACVD), we were able to obtain a highly sensitive and selective H_2 sensor, with low operating temperature.

Table 1. Summary of some characteristics of H_2 sensors based on Pd/PdO nanoparticles functionalized metal oxide nanostructures reported in this work and in the literature. Selected parameters are pointed in [a].

Structure	MOX host matrix	MOX/M NPs	Synthesis Steps	T_{Op} (°C)	Conc. (ppm)	response	Rf/Rnf	Selectivity test	Humidity effect studied	Ref.
PdO/WO_3 Nanoneedles	**WO_3**	**PdO**	**2_Step**	**150**	**500**	**1670**	**755**	**Yes**	**Yes**	**This work**
Pd/WO_3 Nanowires	WO_3	Pd	2_Steps	300	1000	3.1	2.21	Yes	No	[20]
Pd/WO_3 nanofibers	WO_3	Pd	More than 3 steps	300	500	30	No	No	No	[41]
Pd/WO_3 Thick film	WO_3	Pd	More than 4 steps	180	200	69	NA	No	Yes	[42]
Pd/WO_3 Thick film	WO_3	Pd	More than 3 steps	200	200	20	NA	No	Yes	[43]
Pd/ZnO nanorodes	ZnO	Pd	More than 4 steps	260	500	1106	110	No	No	[19]
Pd/SnO_2 nanofibers	SnO_2	Pd	More than 4 steps	160	500	2.6	2	Yes	No	[17]
Pd/SnO_2 Thick film	SnO_2	Pd	More than 4 steps	300	600	200	0.6	No	Yes	[18]

[a] MOX/M NPs: metal oxide/metal nanoparticles, T_{Op} : operating temperature, Conc.: Measured concentration. R_f/R_{nf}: relative change of the sensor response obtained with decorated and undecorated metal oxide sensors.

Conclusion

PdO NPs decorated WO_3 NNs were successfully deposited and integrated onto MEMs based gas sensor substrates, using two steps AACVD approach. The sensing layers were directly grown onto the sensor substrate without any intermediate steps for sensor fabrication. Gas sensing

results revealed that decoration with PdO NPs led to the fabrication of a highly sensitive and selective H_2 sensor. It was found that decoration with small amounts of PdO NPs has a great efficiency in increasing sensor responses (S_R) as well as shifting the response maximum (S_R= 1670) towards lower operating temperatures (150 °C).

The sensor becomes able to detect the studied analyte at very low temperature. As a consequence, at temperature near the ambient (50 °C), the response of PdO/WO_3 sensor toward 500 ppm of H_2 was equal to S_R = 23, which is better than that of some promising devices reported in the literature. Finally, humidity measurements showed that PdO/WO_3 NN sensors displayed low-cross sensitivity toward water vapor, compared to bare WO_3 NN sensors. The addition of PdO NPs helps to suppress the effect of humidity on the sensor resistance changes. These results have been explained as a result of the chemical and electronic sensitization effects of PdO NPs onto WO_3 NNs.

ASSOCIATED CONTENT

Supporting Information

Variation of the precursor amount and its influence on the minimum and maximum particle sizes and average size of the resultant Pd particles, HRTEM analysis of the annealed Pd /WO_3 sample, XPS spectrum of the active layer recorded before and after H_2 gas sensing measurements and SEM and XRD results obtained after gas sensing measurements.

Corresponding Author

*E-mail: eduard.llobet@urv.cat

*E-mail: c.blackman@ucl.ac.uk

Acknowledgements

This work is funded in part by MINECO under grant no. TEC2012-32420, by AGAUR under grant no. 2014 SGR 1267. E.L. is supported by the Catalan Institution for Research and Advanced Studies via the ICREA Academia Award. S.V. is supported by the SoMoPro II Programme, cofinanced by the European Union and the South-Moravian Region, via Grant 4SGA8678. CB is a Research Associate of the National Funds for Scientific Research (FRS-FNRS, Belgium).

References

1. Granqvist, C. G. Electrochromic Tungsten Oxide Films: Review of Progress 1993–1998. *Sol. Energy Mater. Sol. Cells* **2000,** *60*, 201–262.
2. Sun, M.; Xu, N.; Cao, Y.; Yao, J.; Wang, E. Nanocrystalline Tungsten Oxide Thin Film: Preparation, Microstructure, and Photochromic Behavior. *J. Mater. Res.* **2000,** *15*, 927–933.
3. Wen, Z.; Wu, W.; Liu, Z.; Zhang, H.; Li, J.; Chen, J. Ultrahigh-Efficiency Photocatalysts Based on Mesoporous Pt–WO_3 Nanohybrids Phys. *Chem. Chem. Phys.* **2013,** *15*, 6773–6778.
4. Annanouch, F.E.; Haddi, Z.; Vallejos, S.; Umek, P.; Guttmann, P., Bittencourt, C.; Llobet, E. Aerosol-Assisted CVD-Grown WO_3 Nanoneedles Decorated with Copper Oxide Nanoparticles for the Selective and Humidity-Resilient Detection of H_2S. *ACS Appl. Mater. Interfaces* **2015,** *7*, 6842–6851.
5. Li, J.; Zhu, J.; Liu, X. Synthesis, Characterization and Enhanced Gas Sensing Performance of WO_3 Nanotube Bundles. *New J. Chem.* **2013,** *37*, 4241–4249.
6. Zhang, H.; Wang, S.; Wang, Y.; Yang, J.; Gao, X.; Wang, L. TiO_2 (B) Nanoparticle-Functionalized WO_3 Nanorods with Enhanced Gas Sensing Properties. *Phys. Chem. Chem. Phys.* **2014,** *16* (22), 10830–10836.
7. Stoycheva, T.; Annanouch, F.; Gràcia, I.; Llobet, E.; Blackman, C.; Correig, X.; Vallejos, S. Micromachined Gas Sensors Based on Tungsten Oxide Nanoneedles Directly Integrated via Aerosol Assisted CVD. *Sens. Actuators, B* **2014,** *198*, 210–218.
8. Dresselhaus, M.; Thomas, I. Alternative Energy Technologies. *Nature* **2001,** *414*, 332–337.
9. Arya, S. K.; Krishnan, S.; Silva, H.; Jean, S.; Bhansali, S. Advances in Materials for Room Temperature Hydrogen Sensors. *Analyst* **2012,** *137*, 2743–2756.
10. Xiang, Q.; Meng, G.; Zhao, H.; Zhang, Y.; Li, H.; Ma, W.; Xu, J. Au Nanoparticle Modified WO_3 Nanorods with their Enhanced Properties for Photocatalysis and Gas Sensing. *J. Phys. Chem. C* **2010,** *114*, 2049–2055.
11. Vallejos, S.; Umek, P.; Stoycheva, T.; Annanouch, F.; Llobet, E.; Correig, X.; De Marco, P.; Bittencourt, C.; Blackman, C., Single Step Deposition of Au and Pt Nanoparticle Functionalized Tungsten Oxide Nanoneedles Synthesized Via Aerosol Assisted CVD, and Used for Fabrication of Selective Gas Microsensor Arrays. *Adv. Funct. Mater.* **2013,** *23*, 1313–1322.

12. Vallejos, S.; Gracia, I.; Figueras, E.; Cané, C. Nanoscale Heterostructures Based on Fe_2O_3@ WO_{3-x} Nanoneedles and their Direct Integration into Flexible Transducing Platforms for Toluene Sensing. *ACS Appl. Mater. Interfaces* **2015,** *7*, 18638–18649.
13. Miller, D. R.; Akbar, S. A.; Morris, P. A. Nanoscale Metal Oxide-Based Heterojunctions for Gas Sensing: a Review. *Sens. Actuator, B* **2014,** *204*, 250–272.
14. Palgrave, R. G.; Parkin, I. P., Aerosol Assisted Chemical Vapor Deposition using Nanoparticle Precursors: a Route to Nanocomposite Thin Films. *J. Am. Chem. Soc.* **2006,** *128*, 1587–1597.
15. Liu, B.; Cai, D.; Liu, Y.; Wang, D.; Wang, L.; Wang, Y.; Li, H.; Li, Q.; Wang, T. Improved Room-Temperature Hydrogen Sensing Performance of Directly Formed Pd/WO_3 nanocomposite. *Sens. Actuators, B* **2014,** *193*, 28–34.
16. Kukkola, J.; Mohl, M.; Leino, A.-R.; Mäklin, J.; Halonen, N.; Shchukarev, A.; Konya, Z.; Jantunen, H.; Kordas, K. Room Temperature Hydrogen Sensors Based on Metal Decorated WO_3 Nanowires. *Sens. Actuators, B* **2013,** *186*, 90–95.
17. Wang, Z.; Li, Z.; Jiang, T.; Xu, X.; Wang, C., Ultrasensitive Hydrogen Sensor Based on Pd0-loaded SnO_2 Electrospun Nanofibers at Room Temperature. *ACS Appl. Mater. Interfaces* **2013,** *5*, 2013–2021.
18. Suematsu, K.; Shin, Y.; Hua, Z.; Yoshida, K.; Yuasa, M.; Kida, T.; Shimanoe, K. Nanoparticle Cluster Gas Sensor: Controlled Clustering of SnO_2 Nanoparticles for Highly Sensitive Toluene Detection. *ACS Appl. Mater. Interfaces* **2014,** *6*, 5319–5326.
19. Chang, C.-M.; Hon, M.-H.; Leu, I.-C. Outstanding H_2 Sensing Performance of Pd Nanoparticle-Decorated ZnO Nanorod Arrays and the Temperature-Dependent Sensing Mechanisms. *ACS Appl. Mater. Interfaces* **2012,** *5*, 135–143.
20. Chávez, F.; Pérez-Sánchez, G.; Goiz, O.; Zaca-Morán, P.; Peña-Sierra, R.; Morales-Acevedo, A.; Felipe, C.; Soledad-Priego, M., Sensing Performance of Palladium-Functionalized WO_3 Nanowires by a Drop-Casting Method. *ACS Appl. Mater. Interfaces* **2013,** *275*, 28– 35.
21. Ling, M.; Blackman, C. Growth Mechanism of Planar or Nanorod Structured Tungsten Oxide Thin Films Deposited Via Aerosol Assisted Chemical Vapour Deposition (AACVD). *Phys. Status Solidi C* **2015,** *12*, 869–877.
22. Stoycheva, T.; Vallejos, S.; Blackman, C.; Moniz, S.; Calderer, J.; Correig, X. Important Considerations for Effective Gas Sensors Based on Metal Oxide Nanoneedles Films. *Sens. Actuators, B* **2012,** *161*, 406–413.
23. Ma, N.; Suematsu, K.; Yuasa, M.; Shimanoe, K. Pd Size Effect on the Gas Sensing Properties of Pd-Loaded SnO_2 in Humid Atmosphere. *ACS Appl. Mater. Interfaces* **2015,** *7*, 15618–15625.
24. Annanouch, F. E.; Vallejos, S.; Stoycheva, T.; Blackman, C.; Llobet, E., Aerosol Assisted Chemical Vapour Deposition of Gas-Sensitive Nanomaterials. *Thin Solid Films* **2013,** *548*, 703–709.
25. Annanouch, F.; Gràcia, I.; Figueras, E.; Llobet, E.; Cané, C.; Vallejos, S., Localized Aerosol-Assisted CVD of Nanomaterials for the Fabrication of Monolithic Gas Sensor Microarrays. *Sens. Actuators, B* **2015,** *216*, 374–383.
26. Vallejos, S.; Stoycheva, T.; Umek, P.; Navio, C.; Snyders, R.; Bittencourt, C.; Llobet, E.; Blackman, C.; Moniz, S.; Correig, X., Au nanoparticle-Functionalised WO_3 Nanoneedles and their Application in High Sensitivity Gas Sensor Devices. *Chem. Commun.* **2011,** *47*, 565–567.

27. Navío, C.; Vallejos, S.; Stoycheva, T.; Llobet, E.; Correig, X.; Snyders, R.; Blackman, C.; Umek, P.; Ke, X.; Van Tendeloo, G., Gold Clusters on WO_3 Nanoneedles Grown via AACVD: XPS and TEM Studies. *Mater. Chem. Phys.* **2012,** *134*, 809–813.
28. Babaei, A.; Jiang, S. P.; Li, J. Electrocatalytic Promotion of Palladium Nanoparticles on Hydrogen Oxidation on Ni/GDC Anodes of SOFCs via Spillover. *J. Electrochem. Soc.* **2009,** *156*, B1022–B1029.
29. Kim, K. S.; Gossmann, A.; Winograd, N. X-ray Photoelectron Spectroscopic Studies of Palladium Oxides and the Palladium-Oxygen Electrode. *Anal. Chem.* **1974,** *46*, 197–200.
30. Fleisch, T.; Mains, G. J., Photoreduction and Reoxidation of Platinum Oxide and Palladium Oxide Surfaces *J. Phys. Chem.* **1986,** *90*, 5317–5320.
31. Chiang, Y.-J.; Pan, F.-M. PdO Nanoflake Thin Films for CO Gas Sensing at Low Temperatures. *J. Phys. Chem. C* **2013,** *117*, 15593–15601.
32. Van Tong, P.; Hoa, N. D.; Van Quang, V.; Van Duy, N.; Van Hieu, N. Diameter Controlled Synthesis of Tungsten Oxide Nanorod Bundles for Highly Sensitive NO_2 Gas Sensors. *Sens. Actuators, B* **2013,** *183*, 372–380.
33. Yamazoe, N.; Sakai, G.; Shimanoe, K. Oxide Semiconductor Gas Sensors. *Catal. Surv. Asia* **2003,** *7*, 63–75.
34. Chiang, Y.-J.; Lee, K.-C.; Pan, F.-M. Effects of Pt Decoration on the CO Sensing Reaction Mechanism of PdO Nanoflakes Thin Films. *J. Phys. Chem. C* **2015,** *119*, 17278–17287.
35. Yamazoe, N. New Approaches for Improving Semiconductor Gas Sensors. *Sens. Actuators, B* **1991,** *5*, 7–19.
36. Sun, Y.; Wang, H. H., High Performance, Flexible Hydrogen Sensors That Use Carbon Nanotubes Decorated with Palladium Nanoparticles. *Adv. Mater.* **2007,** *19*, 2818– 2823.
37. Kolmakov, A.; Klenov, D.; Lilach, Y.; Stemmer, S.; Moskovits, M., Enhanced Gas Sensing by Individual SnO_2 Nanowires and Nanobelts Functionalized with Pd Catalyst Particles. *Nano Lett.* **2005,** *5*, 667–673.
38. Ma, N.; Suematsu, K.; Yuasa, M.; Kida, T.; Shimanoe, K., Effect of Water Vapor on Pd-Loaded SnO_2 Nanoparticles Gas Sensor. *ACS Appl. Mater. Interfaces* **2015,** *7*, 5863–5869.
39. Koziej, D.; Hübner, M.; Barsan, N.; Weimar, U.; Sikora, M.; Grunwaldt, J.-D., Operando X-ray Absorption Spectroscopy Studies on Pd-SnO_2 based Sensors. *Phys. Chem. Chem. Phys.* **2009,** *11*, 8620–8625.
40. Karthigeyan, A.; Gupta, R.; Scharnagl, K.; Burgmair, M.; Zimmer, M.; Sharma, S.; Eisele, I. Low Temperature NO_2 Sensitivity of Nano-Particulate SnO_2 Film for Work Function Sensors. *Sens. Actuators, B* **2001,** *78*, 69–72.
41. Nikfarjam, A.; Fardindoost, S. Fabrication of Pd Doped WO_3 Nanofiber as Hydrogen Sensor. *Polymers* **2013,** *5*, 45–55.
42. Boudiba, A.; Zhang, C.; Umek, P.; Bittencourt, C.; Snyders, R.; Olivier, M.-G.; Debliquy, M. Sensitive and Rapid Hydrogen Sensors Based on Pd–WO_3 Thick Films with Different Morphologies. *Int. J. Hydrogen Energy* **2013,** *38*, 2565–2577.
43. Boudiba, A.; Roussel, P.; Zhang, C.; Olivier, M.-G.; Snyders, R.; Debliquy, M. Sensing Mechanism of Hydrogen Sensors Based on Palladium-Loaded Tungsten Oxide (Pd–WO_3). *Sens. Actuators, B* **2013,** *187*, 84–93.

Graphical abstract

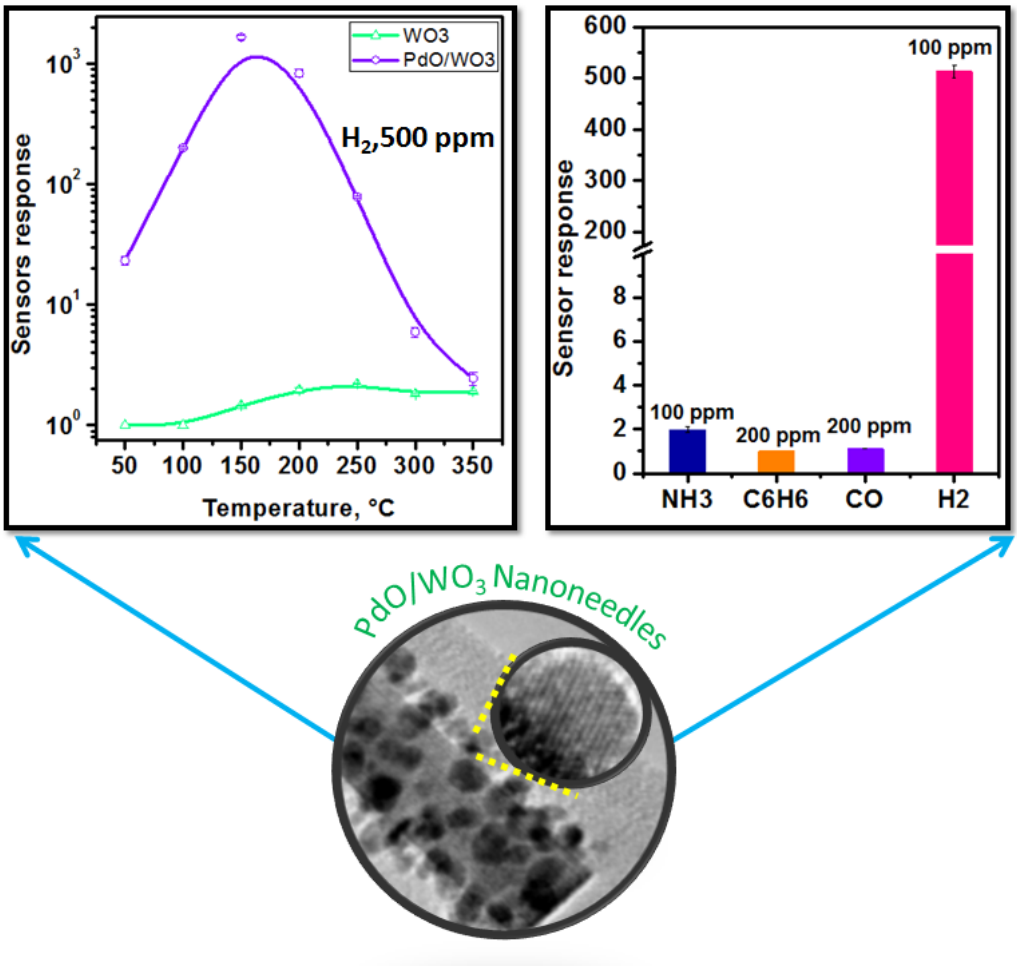

For Table of Contents Only.